



Influence of organic gels on the corrosion of 70/30 cupro-nickel alloy in seawater  
by David Edwin Dobb

A thesis submitted in partial fulfillment of the requirements for the degree of Doctor of Philosophy in  
Chemistry

Montana State University

© Copyright by David Edwin Dobb (1985)

Abstract:

A comprehensive evaluation of the effects of bacto-agar coatings on the corrosion behavior of 70/30 cupro-nickel alloy in seawater is presented. The study provides a data base for isolating physical effects of bacterial caused biofouling layers from their specific chemical effects. Bacto-Agar (Difco, Detroit Mi.) is shown to be a good candidate material to represent a nonviable biofouling layer because of their chemical and physical similarities. Agar layers ranging in thickness from 0 to 60 microns can be reproducibly applied to tubular section samples of the alloy. Once applied, the agar acts primarily as a diffusion barrier to corrosion reactants and products. It will significantly affect the tarnish rate and corrosion product growth morphology if applied prior to corrosion. Its effects are minimal if applied to a sample that has been pre-corroded in excess of one day. The major corrosion parameters considered include specimen geometry, exposure time, flow, seawater chemistry, temperature, and sample pretreatment. Data is presented that systematically evaluates each of these parameters when agar is present and when it is absent. Diffusion of  $\text{OH}^-$  ions generated by the cathodic reduction of  $\text{O}_2$  at the solution-metal interface appears to be the rate controlling factor during initial exposure. Times in excess of one hour show rate dependence from diffusion through the tarnish layer. Appropriate mechanisms are proposed and discussed. In addition, numerous analytical techniques are developed for study of the micro-thin layers at the sample surface. The combination of mass balance and scanning auger analysis is shown to be crucial toward understanding the corrosion process. Procedures for characterization of the microstructure of agar are also presented.

INFLUENCE OF ORGANIC GELS ON THE CORROSION OF  
70/30 CUPRO-NICKEL ALLOY IN SEAWATER

by

David Edwin Dobb

A thesis submitted in partial fulfillment  
of the requirements for the degree

of

Doctor of Philosophy

in

Chemistry

MONTANA STATE UNIVERSITY  
Bozeman, Montana

May 1985

© COPYRIGHT

by

David Edwin Dobb

1985

All Rights Reserved

## STATEMENT OF PERMISSION TO USE

In presenting this thesis in partial fulfillment of the requirements for a doctoral degree at Montana State University, I agree that the Library shall make it available to borrowers under rules of the Library. I further agree that copying of this thesis is allowable only for scholarly purposes, consistent with "fair use" as prescribed in the U.S. Copyright Law. Requests for extensive copying or reproduction of this thesis should be referred to University Microfilms International, 300 North Zeeb Road, Ann Arbor, Michigan 48106, to whom I have granted the "exclusive right to reproduce and distribute copies of the dissertation in and from microfilm and the right to reproduce and distribute by abstract in any format."

Signature David E. Dobb

Date May 15, 1985

## ACKNOWLEDGMENT

I would like to express my sincere gratitude to Dr. Gordon Pagenkopf, my advisor, for his support and helpful guidance during my graduate work, and especially during the past several months. I will always appreciate his patience with this project and my research abilities. His assistance will be kindly remembered. I would also like to express thanks in memory of Dr. Ray Woodriff for his inspiration and confidence in me, for which I will always remember him. Thanks also to the CRISS staff and for their assistance and for the use of the CRISS facilities. Funding for the past year was provided through the MONTS program for which I am very grateful. Special thanks to my wife, Jackie, for her patience and kind understanding over the past few years, and to my parents, brothers and sisters, and fellow graduate students, who have all helped me along the way.

## TABLE OF CONTENTS

	<u>Page</u>
LIST OF TABLES . . . . .	ix
LIST OF FIGURES . . . . .	xi
ABSTRACT . . . . .	xvi
INTRODUCTION . . . . .	1
Uses of Cupro-nickel Alloys . . . . .	1
General Corrosion Behavior . . . . .	7
Impingement: . . . . .	7
Cavitation: . . . . .	8
Crevice Corrosion: . . . . .	9
Pitting: . . . . .	12
Dealloying: . . . . .	16
Stress Corrosion Cracking: . . . . .	16
Sulfidation: . . . . .	17
Fouling: . . . . .	21
Protective Layer Formation . . . . .	25
Importance and Properties: . . . . .	25
Oxide Formation Mechanisms: . . . . .	30
Auger Emission Spectroscopy . . . . .	36
Depth Profiling: . . . . .	41
Other Features: . . . . .	48
Material Balance . . . . .	49
Biofouling and Organic Gel Properties . . . . .	53
Biofouling Processes: . . . . .	53
Biofilm Properties: . . . . .	58
Organic Gel Properties: . . . . .	66
Scope of Study . . . . .	76
EXPERIMENTAL . . . . .	82
Coupon Preparation . . . . .	82
Coupon Pretreatment . . . . .	84

## Table of Contents - Continued

	<u>Page</u>
Corrosion Procedure . . . . .	86
Corrosion Apparatus: . . . . .	86
Corrosion Technique: . . . . .	96
Cleaning and Preparation: . . . . .	96
Corrosion Test: . . . . .	96
Shutdown: . . . . .	100
Agar Coating and Removal . . . . .	100
Coating: . . . . .	101
Removal: . . . . .	104
Auger Analysis Procedure . . . . .	105
General: . . . . .	105
Special Adaptations: . . . . .	109
Data Handling: . . . . .	112
Material Balance Procedure . . . . .	114
General: . . . . .	114
Specific Considerations: . . . . .	116
MATERIAL BALANCE . . . . .	123
Table of Nomenclature . . . . .	123
Derivations . . . . .	125
Weight of Corrosion Product on Coupon, $W_{cp}$ : . . . . .	125
Weight of Oxygen in Corrosion Product, $W_o$ : . . . . .	127
Weight of Cu & Ni in the Corrosion Product, $W_{cu}$ , $W_{ni}$ : . . . . .	132
Metal Lost to Solution, $W_{sc}$ , $W_{sn}$ , $W_{lsc}$ , $W_{lsn}$ : . . . . .	135
Sample Data . . . . .	142
Data Interpretation . . . . .	150
AGAR CHARACTERIZATION EXPERIMENTS . . . . .	156
Bulk Measurements . . . . .	157
Water Absorption and Expansion: . . . . .	158
Diffusion Coefficient Determination: . . . . .	171

## Table of Contents - Continued

	<u>Page</u>
Agar-on-Coupon Characterization . . . . .	186
INFLUENCE OF CORROSION PARAMETERS . . . . .	199
Coupon Pretreatment . . . . .	203
Roughness: . . . . .	204
Degreasing: . . . . .	223
Pickling: . . . . .	226
Annealing: . . . . .	232
Storage: . . . . .	234
Exposure Time . . . . .	235
Solution Losses: . . . . .	260
Flow . . . . .	269
Table of Nomenclature: . . . . .	269
General: . . . . .	272
Flow Characterization Experiments: . . . . .	279
Boundary Layer Equation Derivations: . . . . .	298
Corrosion Rate Prediction: . . . . .	317
Flow Effect Observations and Measurements: . . . . .	324
Temperature . . . . .	336
Water Chemistry . . . . .	352
Salinity: . . . . .	354
Dissolved Oxygen: . . . . .	359
Alkalinity: . . . . .	367
Chlorination: . . . . .	373
Agar Effects . . . . .	376
SUMMARY AND CONCLUSIONS . . . . .	381
LITERATURE CITED . . . . .	389



## LIST OF TABLES

	<u>Page</u>
Table 1. Composition of Cupro-nickel Alloys . . . . .	6
Table 2. Relative Crevice Corrosion Resistance of Metals in Seawater . . . . .	11
Table 3. Measureable Properties of Biofilms . . . . .	59
Table 4. Diffusion Coefficients of Oxygen and Glucose in Various Types of Biofouling Layers . . . . .	65
Table 5. Radius of Pores in Agars and Gelatins for Various Nonelectrolytes (nm) . . . . .	72
Table 6. Flow Rates and Reynolds Numbers Available with Calibrated Flow Restrictors . . . . .	93
Table 7. Base Corrosion Conditions and Variable Ranges . . . . .	98
Table 8. Seawater Samples and Their Salinities . . . . .	99
Table 9. Auger Analysis Conditions . . . . .	107
Table 10. Argon Ion Sputter Beam Conditions . . . . .	107
Table 11. Multiplex Data Parameters . . . . .	108
Table 12. Optimized Atomic Absorption Conditions for Cu, Ni, Fe, and Mn . . . . .	118
Table 13. Nomenclature for Material Balance Equations 15 - 48 . . . . .	123
Table 14. Varied Corrosion Conditions for Mass Balance Experiment . . . . .	144
Table 15. Raw Mass Balance Data Set 1 . . . . .	145
Table 16. Raw Mass Balance Data Set 2 . . . . .	146
Table 17. Mass Balance Data Set 3 . . . . .	147

## List of Tables - Continued

	<u>Page</u>
Table 18. Mass Balance Data Trends . . . . .	148
Table 19. Bulk Agar Water Equilibration Data . . . . .	162
Table 20. Self Diffusion Coefficients of Major Seawater Ions and Pertinent Corrosion Species in Agar . . . . .	182
Table 21. Initial Color Changes of Corroding 70/30 Cupro-nickel Coupons Under Base Conditions . . . . .	201
Table 22. Polishing Grits and Resulting Scratch Widths . . . . .	207
Table 23. Normalized Corrosion Rate Data in $\mu\text{g cm}^2 \text{ min}^{-1}$ Versus Exposure Time . . . . .	261
Table 24. Exposure Time Data Trends Extracted From Table 18 . . . . .	261
Table 25. Nomenclature For Flow Equations 63 - 99 . . . . .	269
Table 26. Characteristic Flow Data for the Tubular Flow Apparatus . . . . .	296
Table 27. Constants for Evaluation of the Zero Order Hyperbolic Bessel Function . . . . .	307
Table 28. Limiting Ionic Conductances in Water at $25^\circ\text{C}$ . . . . .	342
Table 29. Apparent Activation Energy Values in the $0$ to $50^\circ\text{C}$ Temperature Range . . . . .	347
Table 30. Hydrodynamic and Diffusion Barrier Thicknesses Versus Temperature . . . . .	349
Table 31. Diffusion Velocities Versus Temperature . . . . .	350
Table 32. Seawater Analyses . . . . .	353

## LIST OF FIGURES

	<u>Page</u>
Figure 1. Corrosion Rates of Selected Copper Alloys . . .	3
Figure 2. Corrosion Pit Showing Autocatalytic Processes . . . . .	14
Figure 3. Relative Fouling Behavior of Cupro-Nickel Alloys . . . . .	24
Figure 4. Relative Tarnish Rate Versus Flow for 70/30 Cu/Ni in 12.8 g/L Instant Ocean . . . . .	34
Figure 5. 70/30 Cu/Ni Corroded Surface at 1000X Magnification Showing a Uniform Layer Under Turbulent Flow . . . . .	35
Figure 6. Electronic Origin of Auger Electrons . . . . .	37
Figure 7. Typical Auger General Survey . . . . .	39
Figure 8. General Types of Auger Depth Profiles . . . . .	46
Figure 9. Biofilm Growth Stages . . . . .	54
Figure 10. Biofilm Thickness Versus Time for Glass and Aluminum Tubular Specimens . . . . .	60
Figure 11. Real Biofilm Density as a Function of Time . . . . .	62
Figure 12. Change in Biofilm Fiber Count and Chemical Oxygen Demand Per Unit Area with Time . . . . .	64
Figure 13. Diffusion in Agar Gels . . . . .	71
Figure 14. Coupon Dimensions . . . . .	82
Figure 15. Simulated Tubular Flow Corrosion Apparatus . . . . .	87
Figure 16. Heating Rate Data for Corrosion Pump . . . . .	91

## List of Figures - Continued

	<u>Page</u>
Figure 17. Stirred Beaker Corrosion Reactor . . . . .	94
Figure 18. Coupon Holder-Clip Design for Auger Analysis . . . . .	110
Figure 19. General Material Balance Procedure Flowchart . . . . .	115
Figure 20. Resin Column Used for Cu and Ni Recovery from Seawater . . . . .	119
Figure 21. Relationship Between Weight of Oxygen (W <sub>o</sub> ) in the Corrosion Product Layer and the Weight of the Corrosion Product (W <sub>cp</sub> ) . . . . .	133
Figure 22. Bulk Agar Weight Gain With Immersion Time . . . . .	160
Figure 23. Bulk Agar Thickness Increase With Immersion Time . . . . .	163
Figure 24. Relationship Between Agar Thickness and Equilibration Time . . . . .	165
Figure 25. Diaphragm Cell Design for Diffusion Coefficient Measurements in Agar . . . . .	171
Figure 26. Diffusion Time Versus Relative Conductance . . . . .	175
Figure 27. Flux Versus Concentration Gradient for Diffusion of 0.100M NaCl Through 2% Agar . . . . .	180
Figure 28. Initial Agar Weight/Volume % Versus Dry Agar Weight Deposited on a Coupon . . . . .	187
Figure 29. Dry Agar Weight on Coupon Versus Wet Agar Weight on Coupon . . . . .	191
Figure 30. Dry Agar Weight on Coupon Versus Wet Agar Thickness on Coupon . . . . .	194
Figure 31. Initial Agar Weight/Volume % Versus Wet Agar Thickness on Coupon . . . . .	195

## List of Figures - Continued

	<u>Page</u>
Figure 32. Micrograph of a 600 Grit Abraded Surface (1000X) . . . . .	206
Figure 33. Micrographs of Partially Sputter Etched 600 grit and 180 Grit Polished Surfaces Superimposed With an Oxide Element Map . .	211
Figure 34. Tarnish Rates at 30 Minute Exposure Versus Roughness . . . . .	214
Figure 35. Tarnish Rate-Roughness Ratios with Increasing Exposure Time . . . . .	217
Figure 36. Relative Tarnish Rates with Various Degreasing Solvents . . . . .	225
Figure 37. Depth Profile From an Uncorroded, $\text{HNO}_3$ Treated 70/30 Cupro-nickel Coupon . . . .	228
Figure 38. Relative Tarnish Rates for Pickling Acid Treated Samples . . . . .	229
Figure 39. Influence of $\text{HNO}_3$ Exposure Time on Tarnish Rate . . . . .	231
Figure 40. Tarnish Layer Growth With Exposure Time, With and Without Agar Coatings . . . . .	237
Figure 41. Micrograph of a 96 Hour Corroded Coupon . .	240
Figure 42. Depth Profile of a 96 Hour Exposed Coupon .	242
Figure 43. Tarnish Layer Growth During the First 24 Hours, With and Without Agar Coating. . . .	245
Figure 44. Parabolic Plot of Tarnish Amount Versus Exposure Time . . . . .	251
Figure 45. Logarithmic Plot of Tarnish Amount Versus Exposure Time . . . . .	251
Figure 46. Coupon Holder Tube Geometry . . . . .	281
Figure 47. Bubble Path Sketches of Flow Patterns Within the Coupon Holder Tube . . . . .	285

## List of Figures - Continued

	<u>Page</u>
Figure 48. Pitot Tube Arrangement for Point Velocity Determination . . . . .	287
Figure 49. Velocity Profile in the Coupon Holder Tube Under Free Discharge Conditions . . . . .	290
Figure 50. Velocity-Drag Measurement Apparatus . . . . .	292
Figure 51. Drag Coefficient for Spheres Versus Reynolds Number . . . . .	294
Figure 52. Laminar Boundary Layer Thickness Constant Versus Point Velocity to Free Velocity Ratio	301
Figure 53. Relationship Between Dimensionless Tubular Flow Quantities for Boundary Layer Calculations . . . . .	305
Figure 54. Hyperbolic Bessel Function Evaluation Graph	308
Figure 55. Boundary Layer Thickness Versus Dimensionless Velocity Ratio . . . . .	310
Figure 56. Flow Rate Versus Hydrodynamic Boundary Layer Thickness Around a Coupon . . . . .	318
Figure 57. Micrographs of Coupons Under Low Flow and Roughened Conditions Without Agar . . . . .	327
Figure 58. Micrographs of Agar Coated Coupons at Various Flows . . . . .	329
Figure 59. Variation of Absolute and Kinematic Viscosities of 10.0g/Kg Seawater With Temperature . . . . .	339
Figure 60. Diffusion Coefficients for Corrosion Species Versus Temperature . . . . .	343
Figure 61. Actual Tarnish Rate Versus Temperature . . . . .	345
Figure 62. Tarnish Rate Versus Salinity of Various Seawaters . . . . .	356
Figure 63. Dissolved Oxygen Versus Tarnish Rate . . . . .	360
Figure 64. Effect of pH on Tarnish Rate . . . . .	364

## List of Figures - Continued

	<u>Page</u>
Figure 65. Potential - pH Plots for Cu and Ni in Seawater . . . . .	365
Figure 66. Tarnish Rate Versus Bicarbonate Alkalinity . . . . .	368
Figure 67. Chlorination Effects Versus Tarnish Rate .	373
Figure 68. Corrosion Rates Versus Total OH <sup>-</sup> Diffusional Thicknesses . . . . .	377

## ABSTRACT

A comprehensive evaluation of the effects of bacto-agar coatings on the corrosion behavior of 70/30 cupro-nickel alloy in seawater is presented. The study provides a data base for isolating physical effects of bacterial caused biofouling layers from their specific chemical effects. Bacto-Agar (Difco, Detroit, Mi.) is shown to be a good candidate material to represent a nonviable biofouling layer because of their chemical and physical similarities. Agar layers ranging in thickness from 0 to 60 microns can be reproducibly applied to tubular section samples of the alloy. Once applied, the agar acts primarily as a diffusion barrier to corrosion reactants and products. It will significantly affect the tarnish rate and corrosion product growth morphology if applied prior to corrosion. Its effects are minimal if applied to a sample that has been precorroded in excess of one day. The major corrosion parameters considered include specimen geometry, exposure time, flow, seawater chemistry, temperature, and sample pretreatment. Data is presented that systematically evaluates each of these parameters when agar is present and when it is absent. Diffusion of  $\text{OH}^-$  ions generated by the cathodic reduction of  $\text{O}_2$  at the solution-metal interface appears to be the rate controlling factor during initial exposure. Times in excess of one hour show rate dependence from diffusion through the tarnish layer. Appropriate mechanisms are proposed and discussed. In addition, numerous analytical techniques are developed for study of the micro-thin layers at the sample surface. The combination of mass balance and scanning auger analysis is shown to be crucial toward understanding the corrosion process. Procedures for characterization of the microstructure of agar are also presented.



## INTRODUCTION

Uses of Cupro-nickel Alloys

Copper and its alloys have been used extensively during the past 60 years for many fresh water and marine applications. Ship hulls and propellers, piping, and condensor tubes are frequently made of copper alloys because of special properties not seen in other metals. Good mechanical workability, excellent electrical and thermal conductivity, and good fouling and corrosion resistance are the main reasons for the widespread acceptance of copper alloys. Fouling and corrosion resistance are the most interesting properties to study from an academic as well as practical standpoint. Fouling resistance is assisted by the release of cupric ions as corrosion products during corrosion.  $\text{Cu}^{+2}$  has been shown to be toxic to marine organisms that attach to the metal surface.<sup>1</sup> Even if a resistant species gains a "foothold", it will eventually be swept away because of a buildup of nonadhering, nonprotective corrosion products such as paratacamite ( $\text{Cu}_2(\text{OH})_3\text{Cl}$ ) or cupric hydroxide ( $\text{Cu}(\text{OH})_2$ ) between the organism and the metal surface.<sup>2</sup>

Actual metal loss due to corrosion is low, on the order

of 0.001 ipy (inches per year) in quiet seawater for 70/30 and 90/10 cupro-nickels. Both alloys have been exposed in service to seawater for periods of 14 to 16 years and still exhibited a similar low corrosion rate.<sup>3</sup> Figure 1, A-D, summarizes the applications of many copper alloys and their corrosion rates in seawater.

Figure 1A shows corrosion rate data in mils per year for one year immersion tests of copper alloys used as condenser tubing and other heat transfer applications. Each alloy was tested for loss of tensile strength, weight loss, degree of impingement (erosion), and pitting susceptibility in clean, flowing seawater. The close grouping of points for a given alloy indicates a very dependable material while badly scattered data indicate the alloy would be a poor choice for seawater applications. The data indicate that the 70/30 cupro-nickel alloy containing higher Fe levels (0.42%) is superior to all other alloys tested.

Figure 1B shows the same type of corrosion data for copper and certain bronzes high in copper. The usefulness of the materials depend on the conditions of service. For example, if the metal is to be used under low velocity flow conditions, the rate of impingement data can be ignored. The data show Duronz IV (95%Cu, 5%Al, 0.25%As) to be most suitable in general seawater applications, especially if impingement effects are unimportant. Duronz V (98%Cu, 2%Si) shows the poorest performance of all of the alloys tested,

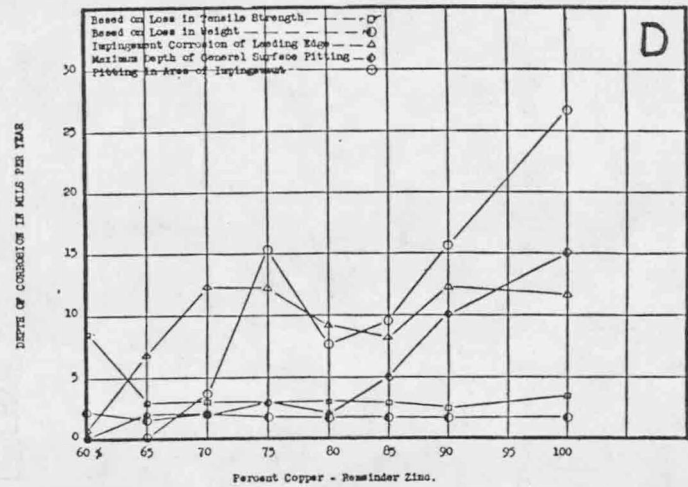
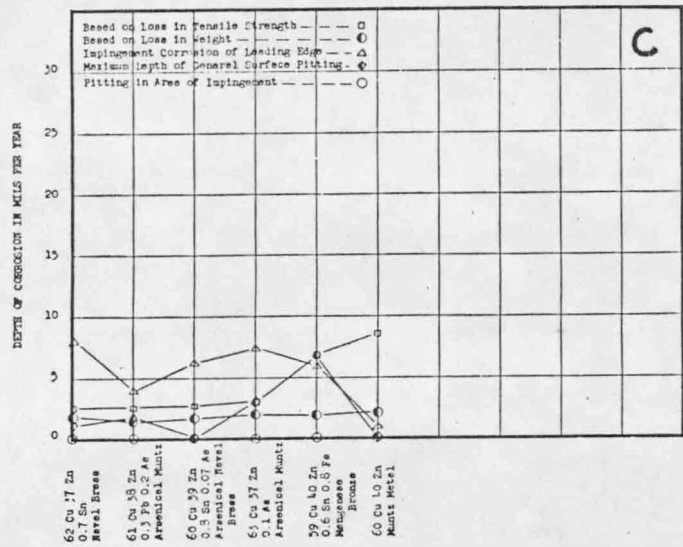
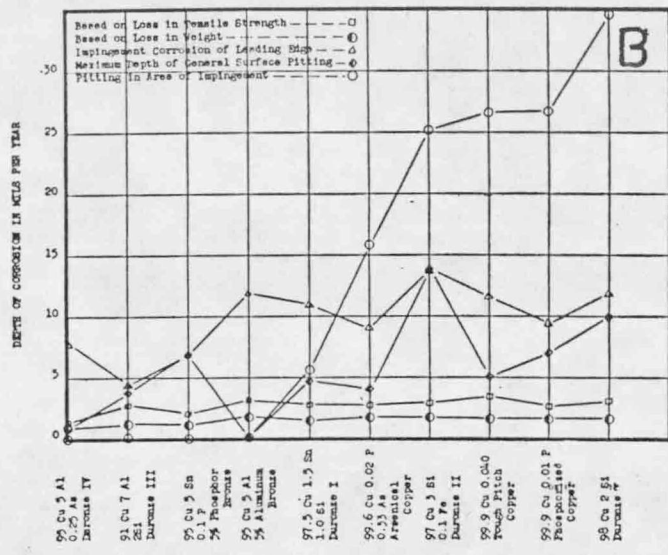
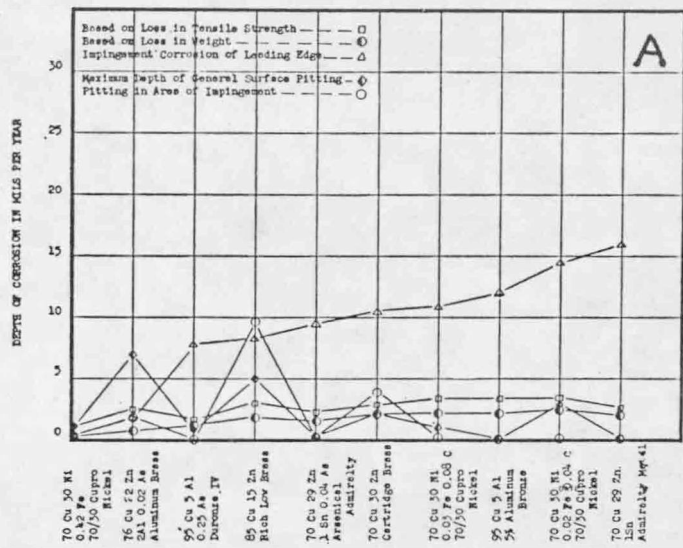


Figure 1. Corrosion Rates of Selected Copper Alloys.4

as indicated by the high point scatter and elevated rates for all of the corrosion types.

Figure 1C shows data for modified Muntz (60%Cu,40%Zn) and other brasses containing alloy modification metals such as As, Sn, and Pb. Arsenical Muntz (63%Cu,37%Zn,0.1%As) shows the best dependability of this group of copper alloys. Muntz metals find more use in condensor systems for fresh water (Great Lakes) applications than in seawater systems. Most of the alloys in this group are especially susceptible to dealloying or dezincification, which will be discussed shortly. As the zinc content increases, the rate of dezincification and sensitivity to stress corrosion cracking increase while the rate of impingement attack decreases. Low zinc levels (<15%), additions of 1% tin, or a few hundredths percent As, Pb, or P, will provide enough dealloying immunity for the metal to be useful in seawater. Easy machinability and corrosion resistance make these alloys a more economical choice for prolonged use than nonalloyed copper.

Figure 1D presents data for Cu-Zn alloys without alloying additions. The alloy containing 60% Cu appears to be most suitable, especially if tensile strength degradation is unimportant as in condensor tubing and water transport applications. Nonalloyed copper shows very poor seawater corrosion behavior, but is still used because it is the least expensive and can be easily machined.

The corrosion resistance of a copper alloy depends on the presence of a surface oxide film which protects the metal from the corrosive environment. The film is mainly composed of  $\text{Cu}_2\text{O}$ <sup>5</sup> which can contain significant levels of alloying metals that give the film its special corrosion-proof properties. The main alloying metal of interest to this study is nickel. Cupro-nickel alloys are the most resistant of the copper alloys, especially in marine applications, due to doping of the  $\text{Cu}_2\text{O}$  lattice with  $\text{Ni}^{++}$  ions. The  $\text{Ni}^{++}$  ions appreciably lower the electrical and ionic conductivity of the protective film, making it more protective against electrochemical activity. Other metals such as Fe and Mn are frequently added to the alloy to assist nickel's incorporation into the oxide lattice and provide a more protective layer. This synergistic effect of Fe and Ni in  $\text{Cu}_2\text{O}$  layers occurs at less than 1% added Fe without much benefit at higher levels.<sup>6</sup> Similar benefits are seen when Fe is added as ferrous sulfate to the corroding solution<sup>7,8</sup> or from Fe released as corrosion products from upstream components. Whether the protective mechanism is the same for the two Fe sources is not known.

Table 1 lists the composition of two of the most popular cupro-nickel alloys as determined by metal dissolution in nitric acid followed by Atomic Absorption Spectrophotometry (AA) of the diluted acid solutions. The samples were commercially obtained tubes from Olin, (East Alton, Ill).

Table 1. Composition of Cupro-nickel Alloys

Alloy	%Cu*	%Ni	%Fe	%Mn	%Zn	%Other
CDA706**	88.0	10.3	1.20	0.40	0.03	0.07
CDA715	68.6	29.7	0.55	0.59	0.09	0.47

\* Weight Percent

\*\* Copper Development Association Number

Alloys CDA706 and CDA715 will hereafter be referred to as 90/10 and 70/30 cupro-nickels, respectively. Most of the work in this study was performed on 70/30 alloy with a very limited amount of research on the 90/10 alloy. The 90/10 alloy is the subject of a similar on-going research task.<sup>9</sup> Based on the discussion so far, it can safely be assumed that a study of the environmental effects on the growth of a protective oxide layer on cupro-nickel alloys used for condenser applications will be of utmost economic importance and will be the topic of a subsequent chapter.

A more detailed account of the behavior and uses of copper alloys in seawater can be found in references 3, 10, and 11. Reference 3 describes general corrosion behavior as related to Ocean Thermal Energy Conversion (OTEC), and has been very useful throughout this study.

### General Corrosion Behavior

Copper alloys can be attacked in a variety of ways when placed in a seawater environment.<sup>3,10,11</sup> The most common reason for failure is localized attack rather than general metal loss. Localized forms of corrosion include impingement (erosion), crevice corrosion, dealloying, pitting, cavitation, stress corrosion cracking, fouling, and sulfidation. It is possible for all forms to be active at the same time, however, impingement, crevice corrosion, sulfidation, and fouling will be the most significant when using copper alloys for heat transfer applications in seawater.<sup>10</sup>

#### Impingement:

Impingement or erosion corrosion occurs under flow conditions that generate enough surface shear stress to tear away the protective oxide film. Flows in excess of 5-6 M/second will usually be sufficient to cause impingement damage on 70/30 cupro-nickel alloy.<sup>12</sup> Impacts by air bubbles or silt can also remove protective corrosion product layers where contact is most probable, such as at elbows, valves, or around obstructions. The exposed area will usually be small relative to protected areas and will become anodic. Under conditions of small anode to cathode ratio, corrosion products cannot form on the anodic surface and an

active electrochemical cell will be set up. The electrochemically assisted dissolution of the exposed area, plus further mechanical erosion, result in corrosion rates many times larger than those seen in the protected areas. The data in Figure 1A indicate alloys like Admiralty metal (70%Cu,29%Zn,1%Sn), or low iron 70/30 cupro-nickels are especially susceptible, while higher iron 70/30 cupro-nickels (>0.4%Fe) are much more resistant. If an alloy forms a dense, well adhering corrosion product layer, the rate of failure by impingement can be diminished. The rate of impingement failure can also be lowered or eliminated altogether by allowing a protective oxide layer to form before subjecting the alloy to high flow conditions. A comprehensive literature review has been conducted on erosion corrosion of copper-nickel alloys in seawater.<sup>13</sup>

#### Cavitation:

Cavitation corrosion is very similar to impingement and occurs primarily in the same places. Cavitation is caused by gas bubble bursting upon surface contact and results in a torn or damaged oxide layer.<sup>11</sup> The local forces generated by bubble bursting can be significant and more than adequate to penetrate the oxide layer. Although this form of corrosion is uncommon, it can be significant under well aerated conditions, such as when cooling towers are employed. The placement of a degasifying unit upstream of



the affected metal will limit bubble damage. An alloy that resists impingement will also perform better under cavitation conditions.

#### Crevice Corrosion:

Another important cause of localized failure is crevice corrosion. This form of metal loss occurs around protected areas or crevices such as blockages and cracks, or under gaskets or deposits. Crevice corrosion is especially important to this study because the presence of biofouling deposits will promote this form of attack. Two electrochemical processes are responsible for crevice corrosion. When oxygen is depleted under a deposit or in a crevice, while the rest of the metal surface has an adequate supply, the depleted region will become anodic and corrode more rapidly.

This oxygen depletion may be aggravated by aerobic activity in viable biofilm deposits, especially under well aerated conditions. Many rod shaped bacteria such as Pseudomonas, Flavobacterium, Achromobacter and other slime producers are the first to attach and populate a metal surface under aerobic conditions.<sup>14</sup> As the slime layer thickens and picks up silt and corrosion products, O<sub>2</sub> transport to the surface is limited, leading to differential oxygen cells. The most depleted areas become anodic and increased metal loss occurs, resulting in numerous,

overlapping shallow pits in the area.

Copper alloys are not as likely to suffer from this mechanism as steels and high nickel alloys are. The extremely passive behavior of these metals makes them more susceptible to pitting and corrosion types similar to pitting when placed in aerated NaCl solutions. (See the discussion on pitting mechanisms to follow)

Copper alloys are more susceptible to crevice corrosion via a metal-ion concentration cell mechanism. Whenever metal ions are allowed to build up, (such as under a deposit or in a crevice), in contact with the corroding metal, that metal will become enobled. This behavior can be described by the Nernst equation for electrochemical activity:

$$E = E^{\circ} - (RT/nF)\ln A_{m^{+n}} \quad (1)$$

E is the actual potential of the metal in contact with the metal ion,  $E^{\circ}$  is the standard electrode potential for the reaction  $M \longrightarrow M^{+n} + ne^{-}$ , R is the universal gas constant, T is the absolute temperature, F is Faraday's constant, and  $A_{m^{+n}}$  is the activity of the metal ion. By the equation, if the metal ion concentration increases, the activity will increase causing E to become more negative than the standard electrode potential. This is a more noble direction in standard electromotive force tables<sup>15</sup> for anodic dissolution. Since the metal in a crevice is in contact with its own ions, it will become more noble, whereas areas outside the crevice will be in contact with

fewer metal ions and will become more anodic. Dissolution of metal will occur in areas adjacent to the crevice where the metal ion levels diminish. High flow tends to accelerate this form of attack by causing higher metal ion concentration gradients near a crevice or deposit. The potential difference given by the Nernst equation will increase with the increasing concentration gradient and anodic activity or metal dissolution must increase. Also, high flow shear forces can strip off patches of biofilm or other deposits, setting up new crevice corrosion sites where metal ion and oxygen concentration cells can develop. This is of particular concern to this study. Table 2 indicates the relative resistance of selected metals against crevice corrosion.

Table 2. Relative Crevice Corrosion Resistance of Metals in Seawater.<sup>16</sup>

Excellent	Very Good	Good	Fair	Poor
Titanium*	90/10 Cu/Ni	H.S.M.Cu	Copper	Type 304 SS <sup>+</sup>
	Aluminum	Admiralty	Arsenical Copper	Type 316 SS
	Bronze	Aluminum Brass		Type 400 SS
		70/30 Cu/Ni		

\* low temperature

+ stainless steel

If fouling or equipment design causes numerous crevice corrosion sites, alloys to the left in the table should be used. Alloys to the right in the table should not be used in seawater, particularly when conditions favor fouling. Type 304 stainless steel (19%Cr,9%Ni,2%Mn,rest Fe), Type 316 SS (17%Cr,12%Ni,2%Mn,0.3%Mo,rest Fe), and Type 400 stainless (17%Cr,1%C,Mn,Si) are especially susceptible to crevice corrosion in seawater mostly because of the aggressive nature of  $\text{Cl}^-$  ions toward all ferrous alloys. The highly passive nature of stainless steel and high Ni alloys coupled with increased reactivity with the chloride ion are conditions that promote both crevice corrosion and pitting. The actual mechanisms of crevice corrosion and pitting are somewhat similar, the main difference being the size of the affected area. Pitting is highly localized while crevice corrosion affects large areas, depending on the size of the crevice. Both types are frequently encountered together.

#### Pitting:

Pitting is not usually a problem with copper alloys in seawater,<sup>16</sup> as long as the right alloy is matched to the service conditions. Susceptibility to pitting attack for various copper alloys is shown in Figure 1. Muntz metal (60%Cu,40%Zn) and other noninhibited Cu/Zn alloys are more subject to pitting than are the condenser tube alloys. Pitting also increases as the nickel content is raised.

Methods of measuring pit depths and conditions for formation have been studied. A scanning microprobe potentiometer<sup>17</sup> has been used to measure potential differences near pits and map active pits or possible pitting sites across the surface of a corroding metal. The method is more accurate than the usual optical microscopy method of studying pits which is slower and more tedious. Since pitting causes failure as soon as one pit penetrates through the metal, the determination of the growth rates of only the deepest pits is of concern. The search for the deepest pits is tedious and often misleading, thus making prediction of pitting behavior more difficult.

Whether or not a pit can form depends on the metal and the degree of reactivity of the protective corrosion product layer. Metals with extremely inert layers on the surface coupled with inherent reactivity with the  $\text{Cl}^-$  ion, such as stainless steels and high nickel alloys, are especially susceptible to pitting. The exact reason for this behavior is somewhat complex, and the process illustrated in Figure 2 is simplified. The figure shows a metal exposed to an aerated sodium chloride solution.

Pitting corrosion is an autocatalytic process, where corrosion reactions within an existing pit produce conditions that are self-stimulating and self-propagating towards continued growth of the pit. Rapid growth and catastrophic failure are the result.



The formation of metal chlorides by Step 2 tends to accelerate Step 1 and an anodic current develops. Adjacent areas, where  $O_2$  reduction takes place, must become cathodic and what is called an active-passive cell develops. If the cell is sufficiently active, a surplus of positive metal ions will develop and  $Cl^-$  ions will migrate to the vicinity to balance charges. The newly formed metal chlorides can hydrolyze by Step 3 to form insoluble hydroxides and hydrochloric acid which further accelerates corrosion. If the pit becomes deep enough, the effects of flow cannot dilute the hydrochloric acid by mixing and thus the concentration raises. The density of the pit solution will be greater than the surrounding salt water and will increase towards the bottom of the pit. This explains why pits grow faster in the direction of gravity. Formation of  $HCl$  promotes further metal dissolution which in turn makes more  $HCl$ . It is easy to see why the process is autocatalytic.

Potential differences within an active-passive cell have been measured up to  $0.5V$ .<sup>10</sup> At potentials this large, a pit will actually cathodically protect the metal for some distance away. This will lead to the worst kind of pitting where there are few, very deep, and rapidly growing pits. The best defense against pitting is to choose an alloy that is proven resistant to pitting in a given environment. Alloys that form an oxide layer that is not completely "passive" or alloys that are not very reactive with chloride

ions (high copper alloys), will be resistant to pitting in seawater.

#### Dealloying:

Dealloying of cupro-nickels is not a problem as long as temperatures are kept low ( $<100^{\circ}\text{C}$ ). Although condensor alloys rarely experience temperatures above  $100^{\circ}\text{C}$ , local "hot spots" may exist, causing dealloying and possible local failure if the process penetrates the metal. Copper-zinc alloys (brasses) are the most susceptible of the copper alloys to dealloying or specifically, dezincification. The exact mechanism is largely unresolved, but there is evidence that zinc diffuses to the alloy surface faster than copper and reacts there preferentially to be lost to solution. A copper rich alloy residue with little mechanical strength is left behind in a uniform "layer" type or localized "plug" type of dealloying. Pipe splitting and perforation are the usual result. Addition of inhibitors like Al, Sb, Sn, Pb, and P, or lowering the zinc ( $<15\%$ ) content will slow Zn diffusion and solve dezincification problems.

#### Stress Corrosion Cracking:

This form of localized corrosion occurs when a metal is placed in tensile stress in a specific environment. Minute cracks form at the surface and accelerate intergranularly until penetration through the metal occurs,



causing failure. Copper alloys (especially brasses) in tension will crack if exposed to  $\text{NH}_3$  or nitrogen oxides in the presence of oxygen and moisture. The problem is frequently encountered with telephone equipment exposed to urban atmospheres, especially in Los Angeles where higher levels of nitrogen oxides occur.<sup>10</sup>

The most favored mechanism for stress corrosion cracking involves adsorption of complexing species from the environment which weakens the cohesive bonds between surface metal atoms. If the metal is under tensile stress, there is an increasing tendency for a crack to develop. Cohesive forces are then disrupted at the crack tip where new complexing species can penetrate, causing the crack to grow. Stress corrosion cracking is rarely encountered for copper alloys used in condensor applications because tensile stresses are low and the specific atmosphere required for crack growth is uncommon. Since stress corrosion cracking has little relevance to the theme of this study, it will not be covered in more detail. Reference 10, pages 312-320 has a detailed discussion on stress corrosion mechanisms.

#### Sulfidation:

Sulfidation is one of the more serious localized corrosion problems for condensor alloys. The breakdown in structure and passivity of existing oxide layers is responsible. Sulfur enters the oxide layer as  $\text{S}^{-2}$  ions,

substituting for  $O^{-2}$ , which raises the ionic and electrical conductivity. This offers lowered resistance to anodic (metal-dissolution) reactions and the corrosion rate increases. The protective layer develops numerous defects and pores, allowing the corrosive environment to reach fresh metal. 90/10 and 70/30 cupro-nickel will experience accelerated localized corrosion when exposed to sulfide levels as low as 0.01 mg/l for a few days.<sup>18</sup> The effects of this sulfide exposure will be seen for several months after the metal is placed in sulfide-free seawater. Sulfide occurs in seawater as a product of decay of marine organisms, plant tissues, and other coastal debris that contain organically-bound sulfur. The oxidation of organic matter during decay can also deplete the seawater's oxygen, leading to anaerobic conditions. Anaerobic sulfate-reducing bacteria like Sporovibrio desulfuricans can thrive and reduce naturally occurring sulfate salts in seawater to sulfides. Other sources of sulfide include municipal sewage discharge, with its well known rotten-egg smell ( $H_2S$ ), polluted rivers, and  $SO_2$  contaminated coastal air.

Ammonia is also found in this type of environment and is known to accelerate corrosion by forming strong, soluble complexes with Cu. An extensive review of cupro-nickel applications in ammoniacal environments is presented in Reference 3 which discusses the use of cupro-nickel alloys as candidate materials for OTEC heat exchangers.

If sulfide species are present, the seawater must contain low levels of oxygen, since sulfides are rapidly oxidized. A sulfide half-life of only 20 minutes in aerated seawater has been observed.<sup>19</sup> Actual metal oxidation rates are very low in anaerobic, sulfide polluted waters due to supply limitations on the cathodic oxygen reduction reaction. Although oxidation rates are low, the rate of weight loss for 70/30 and 90/10 cupro-nickels increases by an order of magnitude in the presence of sulfide over the rate seen in sulfide-free deoxygenated seawater. The reason for the accelerated corrosion rate is due to a significant shift in the corrosion potential to the -0.45 to -0.72 V (SCE) range when cupro-nickels are placed in sulfide polluted, anaerobic seawater. This shift is sufficient to allow hydrogen ion reduction as a new cathode reaction. Anodic metal dissolution can then be supported at an accelerated rate. The growth of highly defective  $\text{Cu}_2\text{S}$  as the primary corrosion product replaces the normally protective  $\text{Cu}_2\text{O}$  layer. If oxygen is brought to the surface by higher flow rates<sup>20</sup> or the incoming tide, corrosion rates soar because oxygen reduction can occur without formation of a protective  $\text{Cu}_2\text{O}$  layer.  $\text{Cu}_2\text{O}$  is prevented from forming in the presence of existing  $\text{Cu}_2\text{S}$ , which is nonprotective.

The anodic dissolution of metal can occur unabated at defects and pores in the  $\text{Cu}_2\text{S}$  layer resulting in localized corrosion damage. Even if protective  $\text{Cu}_2\text{O}$  does form,

anaerobic sulfide polluted conditions can return when the tide goes back out causing more  $\text{Cu}_2\text{S}$  formation. It is alternate exposure to anaerobic, sulfide polluted seawater that is responsible for the high corrosion rates of cupro-nickel naval equipment operating in coastal areas.<sup>21,22</sup> Localized corrosion rates as high as 19 mm/year have been measured.<sup>23</sup>

It has also been proposed that sulfide oxidation products can be aggressive towards cupro-nickel alloys.<sup>24</sup> Species such as sulfate ( $\text{SO}_4^{2-}$ ), sulfite ( $\text{SO}_3^{2-}$ ), thio-sulfate ( $\text{S}_2\text{O}_3^{2-}$ ), and polysulfides ( $\text{S}_{2-5}$ ) can be formed under aerobic conditions by actions of bacteria such as Thiobacillus thiooxidans, or by the direct reaction of sulfides with dissolved oxygen. When the oxidation products of sulfides encounter the corrosion potentials at the surface of the metal, they can be reduced back to sulfides and contribute in part to the cathode reaction even if oxygen is not present. Any time alternative cathode reactions become possible anodic dissolution currents will increase and corrosion rates will rise.

Other mechanistic and kinetic studies of sulfide effects on cupro-nickels have been performed,<sup>25,26</sup> but are somewhat removed from the theme of this study. Although sulfidation is a very important cause of localized corrosion, its interference with biofilm corrosion activity on cupro-nickels has not been established, or studied here.

Fouling:

Two major problems associated with fouling are lowered heat transfer efficiency and inhibited flow.<sup>14</sup> Both problems are economically important, requiring expense of energy to overcome. Ocean Thermal Energy Conversion (OTEC) systems require maximum heat transfer efficiency to be economical due to the low temperature differences between warmer surface waters and cold, deep waters. Power plant condensor pipes must effectively remove waste heat in order for the system to operate correctly. Heat transfer efficiencies can be lowered as much as 50% by a deposit layer only 250 um thick due to the layer's insulating properties.<sup>27</sup> Reduced flow due to blockage by films and debris also lowers heat transfer efficiencies because of cooling water supply problems. Pumping systems must work harder to overcome rougher tube walls and decreased internal diameter. Complete blockage of a pipe can occur in extreme cases.

Causes of these pipe blockages can be grouped into four different categories:<sup>3</sup>

- (1) Corrosion fouling due to growth of corrosion products that are bulky and insulating.
- (2) Biological fouling due to attachment and growth of bacteria, algae, and larger organisms such as mussels and barnacles.

(3) Suspended solids fouling due to silt or other debris that may settle out or become trapped in other fouling layers.

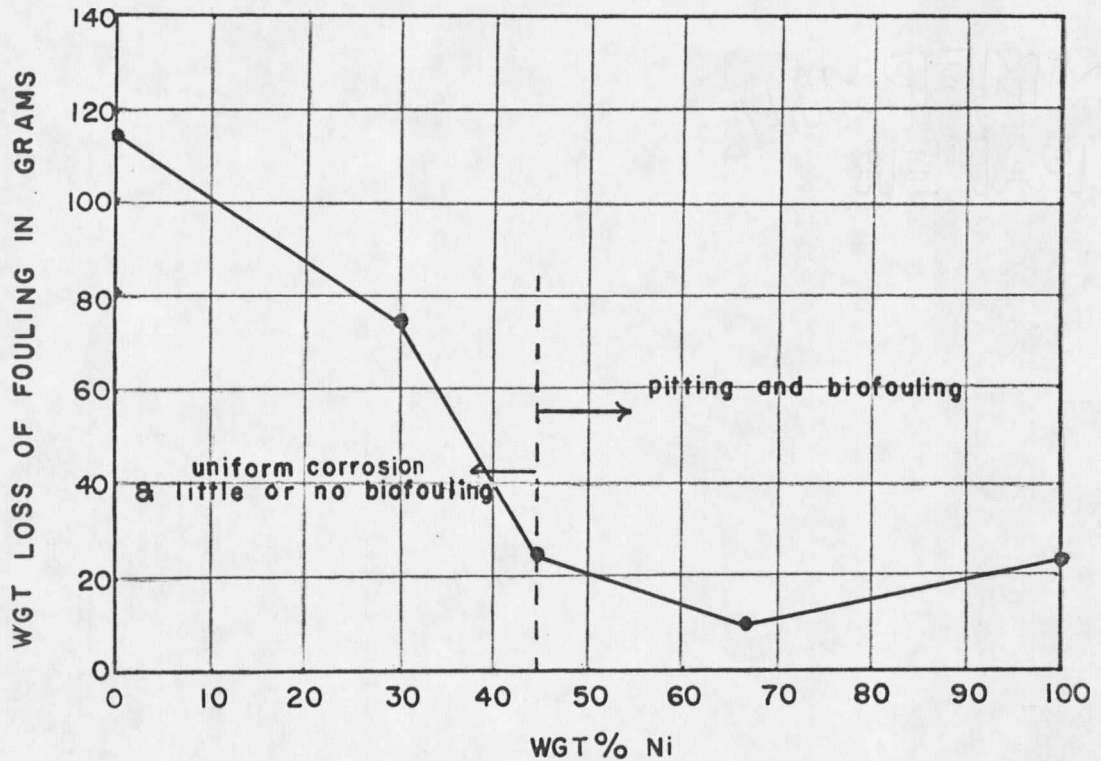
(4) Scale formation fouling due to crystallization of compounds with inverse solubility, i.e., solubility decreases as the temperature is raised. Calcium carbonate, calcium sulfate and other hardness causing ions are mainly responsible.

The first two types are of most concern to this study because of their significant relationship to corrosion. Scale formation fouling, if nonuniform, can promote crevice corrosion by protecting the surface from flow and turbulence, allowing metal ion concentration cells to form. (See previous discussion on crevice corrosion.) The corrosion is due to blockage only since the crystalline scales have little or no corrosive properties of their own. Of more interest is biological fouling due to a blocking effect and active corrosion participation caused by biological activity. This subject will be covered in more detail later.

Fouling control can be accomplished in a variety of ways.<sup>14</sup> Mechanical scouring and chemical methods are routinely used. Chlorine and other oxidizing agents can be particularly effective when closely monitored, but are hazardous and can be expensive. Condensor biocide soaking and antifouling coatings with control released toxic

ingredients have also been tried. Nonchemical methods include flow reversal, heat soaking, irradiation, and ultrasonic vibration. Not generally feasible techniques include osmotic shock, (fresh water is introduced to remove saltwater species), and anoxic water treatment where water is allowed to stagnate and become anaerobic in order to remove aerobic organisms. Generally, mechanical scouring and chlorination are the most effective ways to control fouling.

The best way to prevent fouling is to choose an alloy that is resistant. Fouling tests indicate most copper alloys are resistant and a relationship exists between resistance and alloy composition.<sup>1</sup> 90\10 cupro-nickel alloy and low iron 70/30 cupro-nickel alloys are more resistant to biological fouling than high iron 70/30 cupro-nickel. The corrosion product on the higher iron alloy is more protective and highly adherent, which cuts down on release of toxic cupric ions and sloughing of attached deposits. The less "passive" the corrosion product layer becomes, the more resistant the alloy will be to fouling, however, it will be more susceptible to corrosion. In this regard, a trade-off must occur and high iron 70/30 cupro-nickel (CDA715) will be a good dependable alloy in seawater condensers. Figure 3 shows the relative fouling resistance of some cupro-nickel alloys in terms of amount of biological species such as barnacles and microorganisms that lost their "foothold" to the surface.

Figure 3. Relative Fouling Behavior of Cupro-nickel Alloys,<sup>28</sup>

The data show that low Ni alloys with less passive oxide layers are more resistant to biological fouling. High Ni alloys, especially Monel (70%Ni,30%Cu), are likely to be covered by biological fouling and suffer from increased pitting attack.<sup>10,29,30</sup>

It is hoped that the preceding discussion of the uses and corrosion behavior of copper alloys will aid in identifying the role of biological fouling layers and artificial gel (agar) layers in the corrosion process. Three general references have been most helpful in the development of these areas.<sup>10,11,29</sup>



Protective Layer FormationImportance and Properties:

When a metal is placed in a corroding medium, such as seawater, it will be attacked and consumed unless some form of passivation occurs. Passivation takes place because of a physical blockage of corroding reactants from the surface caused by corrosion product buildup. The study of corrosion product buildup is therefore fundamental to understanding a metal's corrosion resistance.<sup>13,16,31-33</sup>

Good corrosion performance depends on the right choice of metal for a given environment,<sup>11</sup> since a metal will only form protective corrosion products under certain conditions. If conditions are right for ample amounts of corrosion product to form, the metal will generally be protected. However, if the coating material is porous or adheres poorly, it will afford little or no protection.<sup>3</sup> As was mentioned, this condition is common with cupro-nickels exposed to sulfide polluted seawater. The amount of corrosion product formed and its structure are the key elements of study for prediction of good corrosion performance.

Extensive research has been conducted on corrosion products formed on cupro-nickel alloys because of their simplified mathematical treatability and practical implications.<sup>34,35</sup> Copper and nickel are mutually soluble at all concentrations and have nearly the same atomic weight, molar

volume, and crystal structure (body centered cubic). This makes the mathematical treatment of the formation of dual oxide layers much simpler<sup>36</sup> compared to other two metal alloys such as brass or bronze.

The corrosion product layer that forms on the surface of cupro-nickel alloys is considered "passive", which implies nonreactivity. The "passive" description can only be used to indicate a slowing down of the corrosion rate to low levels since the tarnish layer is anything but non-reactive. Oxidation of the surface metal provides a continuous source of protective material which will be soluble to some extent in the corrosive medium. Chloride ions in seawater will cause copper oxides to dissolve while new oxides form at the same time. As a result, the tarnish layer is continually changing thickness and reaches a steady state only after several days. Time exposure studies, which will be shown later, indicate at least three days are required for equilibration of initially formed  $\text{Cu}_2\text{O}$  layers on 70/30 cupro-nickel exposed to seawater. Other tests performed in real seawater service show surface oxide layers will still be equilibrating after 16 years of exposure.<sup>3</sup>

The formation of a protective layer is actually part of the corrosion process and contributes to the overall corrosion rate. Initially, it will add to the rate until it reaches a thickness sufficient to block reactant from fresh metal. After this occurs, further growth actually slows the

overall corrosion rate, making oxide layer formation a beneficial form of corrosion. It is the oxide layer that must withstand the corrosive environment and prevent localized metal loss.

The unusual "passive" behavior of the oxide layer formed on cupro-nickel alloys is responsible for their resistance to macrofouling by mussels and barnacles and microfouling by algae and bacterial slimes. When an organism attaches to the Cu/Ni surface, insoluble, non-adhering corrosion products such as  $\text{Cu}(\text{OH})_2$  or  $\text{Cu}_2(\text{OH})_3\text{Cl}$  build up between the organism and the metal oxide layer. This causes the organism to lose its "foothold" and be swept away under flowing conditions.<sup>37,38</sup> The addition of chlorine for biological film control may also promote the formation of nonadhering corrosion products, hastening the removal of organisms by the above mechanism. This possibility is discussed more specifically in the section on chlorination effects.

The growth of the oxide layer follows several distinct stages before it reaches a steady state with the seawater environment. As soon as the metal is placed in a corroding medium that will allow corrosion product formation, initiation of protective layer growth begins. Growth during this stage is usually rapid due to the thinness of the layer and will taper off parabolically with time according to diffusion theories proposed by Wagner.<sup>39</sup>

If the initial tarnish rate is high enough, damage from impingement or sulfidation can be readily repaired and failure may be prevented. Since impingement and sulfidation are the most common modes of failure for cupro-nickels, the conditions for rapid formation of initial tarnish layers will be most desirable. One of the main topics of this work addressed determination of conditions that allow rapid oxide formation on a short term basis. It was found that warm, well aerated, flowing seawater that has been diluted by fresh water, will promote the most rapid oxide formation. These conditions can be quite common in coastal waters.

After initiation, the corrosion product layer will begin to equilibrate with the environment. Any change in conditions such as establishment of a biofilm or attachment of a macroorganism will cause the passive layer to change its composition and thickness to a new steady state. The corrosion product formed on an alloy must also equilibrate with respect to the individual oxide phases since they may not be mutually soluble. As the phases equilibrate, the scale morphology will change, which may alter the corrosion protection characteristics and growth rate of the passive layer. Completely separate oxide phases with significantly different corrosion protection properties can form on the surface of alloys such as brass and bronze<sup>40</sup> due to solubility differences between Cu, Zn, and Sn oxides.

As has been previously mentioned, oxides on cupro-

nickel alloys have special properties not seen in most other copper alloys. During the equilibration stage, the initially formed  $\text{Cu}_2\text{O}$  layer will become doped with Ni and Fe ions from the alloy, which lowers the electronic and ionic conductivity. Since the rate of the anodic half reaction (metal dissolution) depends on the oxide layer's electrical resistivity, the overall corrosion rate will be stifled as more and more dopant ions enter the  $\text{Cu}_2\text{O}$  lattice. This self-limiting characteristic prevents undue corrosion product formation and limits the overall corrosion rate. Many ferrous alloys do not form corrosion products with this type of self-limitation and continue to form a layer, unchecked, until a "rust through" occurs. For cupro-nickels, this stage will be referred to as the reorganization step.

After reorganization, the rate of growth of tarnish layer slows and becomes equal to the rate of erosion or dissolution of the layer, resulting in a steady state. Cupro-nickel alloys studied in this work rarely, if ever, formed a tarnish layer more than 2000 Angstroms thick. They will reach this steady state in two or three days and show little change unless there is a disturbance such as biofilm growth on the surface. Since the induction period for the attachment of a biofilm is usually within two or three days, depending on surface roughness and nutrient availability,<sup>41</sup> the influence of biofilm attachment will affect the equilibration stage more than the earlier steps. Biofilm effects

should be evaluated on metal samples that have already gone through the initiation and reorganization stages, to give the most realistic data.

#### Oxide Formation Mechanisms:

The formation of a protective corrosion product layer can be described by several mechanisms proposed by Armstrong.<sup>42</sup> The surface film is proposed to grow by a solid-state (SS) pathway or by dissolution-precipitation (DP). The SS mechanism involves migration of cations through existing oxide layer to the surface where they react with adsorbed anions without passing into the corroding solution. The DP mechanism, originally proposed by Müller,<sup>43</sup> is an extension of the SS mechanism whereby the cation passes into the solution near the surface and precipitates with the anion as soon as a critical concentration or supersaturation level is reached. The main difference between the two models is the reaction site of the cation with the anion, SS being at the very surface and DP being very near the surface. The difference is small, thus it is conceivable that both mechanisms can occur simultaneously. However, several tests should indicate which is predominant. The DP mechanism will be significantly affected by flow and bulk fluid turbulence while the SS pathway will not. Complications arise when the SS and DP models appear similar. If the SS mechanism is accompanied by reversible metal

dissolution, flow and turbulence will affect the rate of dissolution and experimental observation will indicate the DP mechanism is occurring. If the DP mechanism is taking place exclusively, flow effects will lower the critical concentration of anions and cations near the surface by diluting ions with bulk fluid. Under higher flow conditions, greater amounts of metal ions will be swept into solution and the tarnish layer growth rate should decrease. Detection of significant levels of cations passing into the bulk fluid will prove the DP mechanism to be occurring only if reversible metal dissolution is absent. If metal dissolution is occurring, it will be difficult to tell if solution species are precursors of a precipitate or from metal solubility. Addition of metal ions to the bulk fluid will slow the dissolution reaction if it is reversible and the Nernst equation will be obeyed. Any other behavior will be evidence for the DP mechanism. If the SS mechanism is dominant, without dissolution complications, the tarnish layer growth rate will be just a function of temperature and availability of anions to the surface.

Precautions must be taken in interpreting flow data to study reaction mechanisms. Flow rates must be sufficient to bring an adequate supply of reactants ( $O_2$ ) to the surface or else the tarnish layer growth rate will be dependent on diffusion control. Once the flow rate increases to cause turbulence, the supply of fresh reactants will no longer be

diffusion controlled and flow effects can be used to determine if the SS or DP pathway is taking place. Even under turbulent conditions, there will be a thin, laminar sublayer<sup>44</sup> next to the surface. Reactants still must diffuse through the boundary to reach the surface. If the surface is too rough, the sublayer will be affected by turbulence and will be more difficult to characterize. Thus, flow effects should be evaluated on smooth walled specimens under turbulent conditions.

When reactions are no longer diffusion controlled, they are considered to be under activation control. The flow needed to change from diffusion to activation control on cupro-nickel alloys in seawater has been characterized.<sup>45</sup> It was determined that the change to turbulent conditions from laminar usually accompanies the reaction transition. The change to turbulent condition can be predicted by Reynolds number calculations using the following equation for tubular flow:

$$R_e = dV/v \quad (2)$$

where  $d$  is the tube diameter,  $V$  is the fluid velocity, and  $v$  is the kinematic viscosity which is  $0.00912\text{cm}^2/\text{sec}$  for seawater. Turbulence usually occurs at  $R_e$  values above 2300.

For this study, 1.45cm diameter tubes were used, making the critical velocity for turbulence around 0.15m/sec to reach a Reynolds number of 2300. Thus, only flows above 0.15m/sec were used to determine whether tarnish reactions



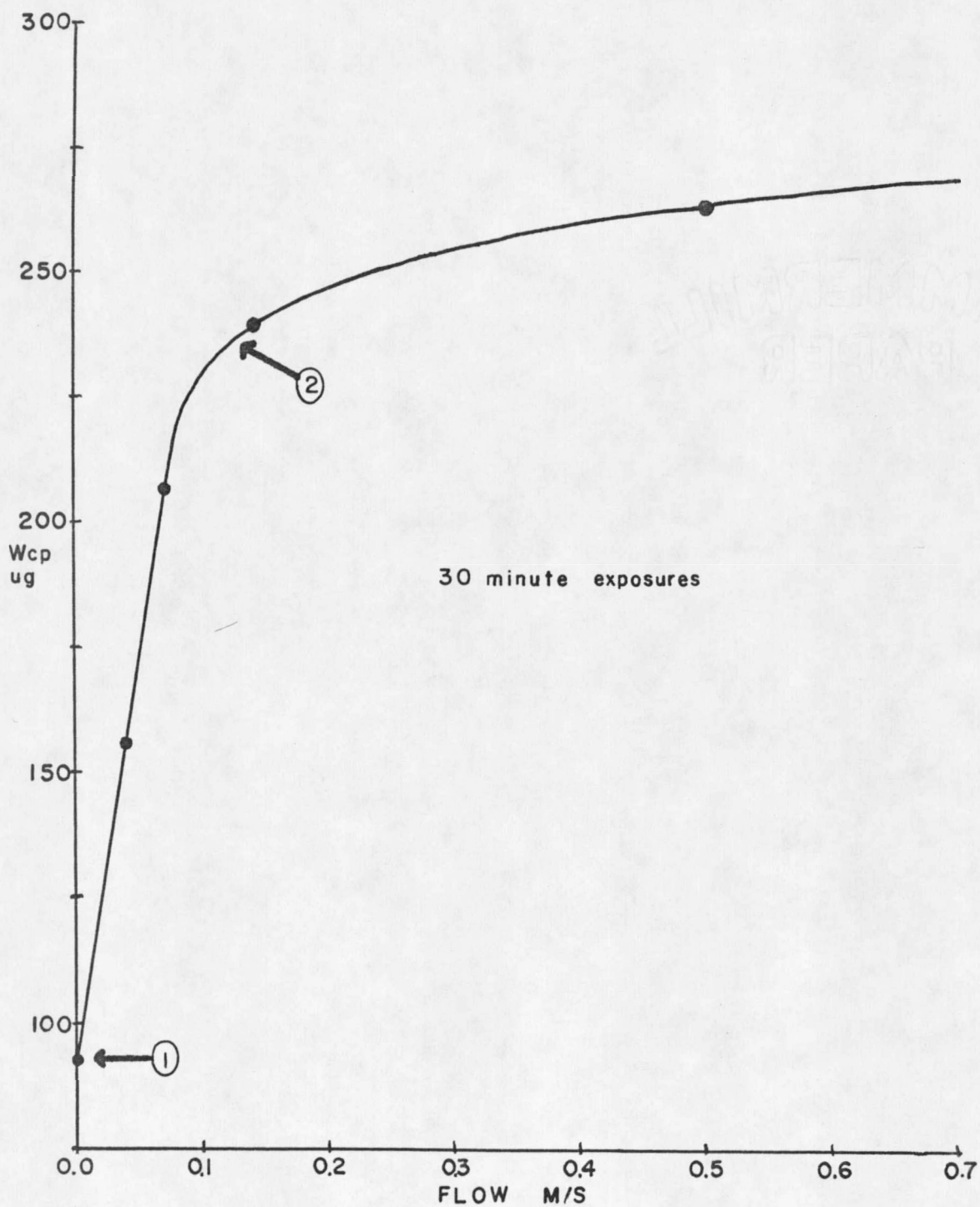
proceed by the DP or SS pathway.

Figure 4 shows the effect of flow on the weight of corrosion product ( $W_{cp}$ ) that formed on 70:30 cupro-nickel in artificial seawater (12.8g/l Instant Ocean, Mentor Ohio) for 30 minute exposure tests.

The onset of activation control should occur above 0.15 m/second flow and diffusion of reactants to the surface should not interfere with flow effect interpretation above this value (Point 2). The effects of diffusion to the surface can be seen in going from Point 1 to Point 2. Point 1 is for purely stagnant conditions where the only way reactants can be brought to the surface is by diffusion. As faster and faster laminar flow brings increasing amounts of  $O_2$  to the metal surface, the corrosion product builds significantly. Once turbulence is reached, above Point 2, further increases in flow cause only slight increases in the corrosion product growth rate. It was mentioned that an increase in flow will lower the rate of tarnish layer growth if the DP mechanism is dominant. Since this is not the case in Figure 4, there is strong evidence the tarnish layer on 70:30 cupro-nickel grows by the SS mechanism, under these conditions.

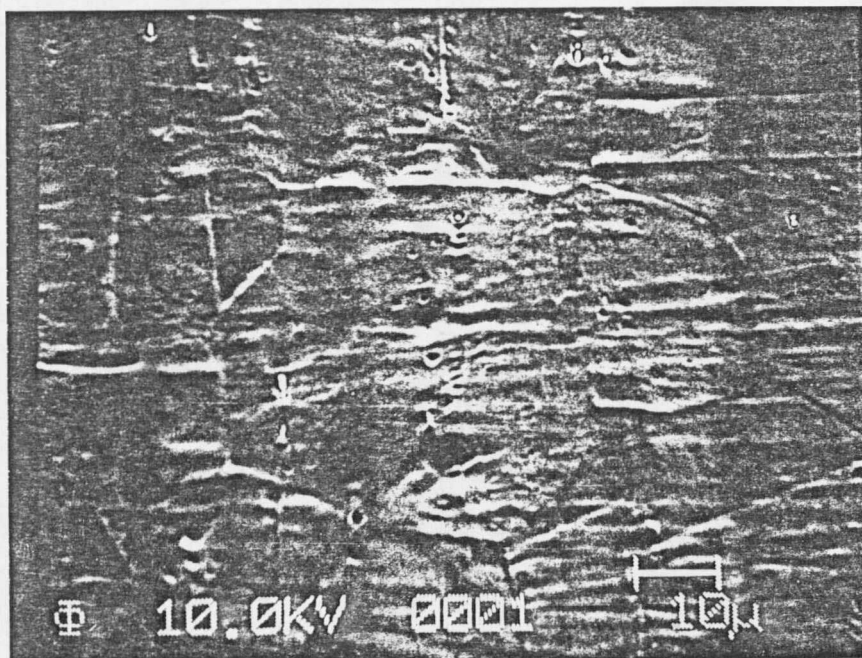
Further evidence that the DP mechanism is not significant lies in the microscopic appearance of the corrosion product layer on the metal samples. Since the DP mechanism is a precipitation process, it will involve

Figure 4. Relative Tarnish Rate Versus Flow for 70/30 Cu/Ni  
in 12.8 g/L Instant Ocean.



nucleation and three-dimensional crystal growth. The layers formed by this mechanism are nonuniform and tarnish layer features such as pores and bumps should be evident. Also, the physical appearance of corroded samples with these features will be dull due to scattered light. Figure 5 shows a micrograph of the corroded 70:30 cupro-nickel sample near Point 2 of Figure 4.<sup>46</sup> The smooth, even tarnish layer shows no features other than underlying metal topography. All samples corroded under conditions given for Figure 4 show high lustre, further indicating a uniform tarnish layer.

Figure 5. 70/30 Cu/Ni Corroded Surface at 1000 X Magnification Showing a Uniform Layer Under Turbulent Flow.



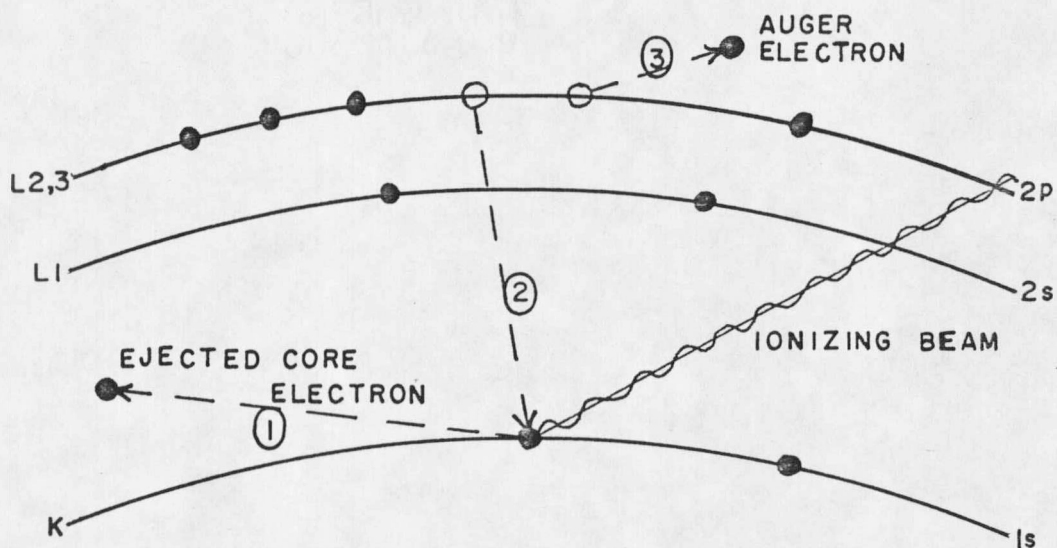
The SS mechanism will involve nucleation and two dimensional growth across the surface until a monolayer is reached.<sup>42</sup> The layer will build in thickness uniformly as metal cations diffuse to the surface and react with adsorbed anions. Based on physical and microscopic appearance, and observed behavior of rates on flow, it can be concluded that the SS path is dominant for oxidation of Cu/Ni in seawater.

#### Auger Emission Spectroscopy

This study made use of Auger Emission Spectroscopy (AES) for direct observation of protective oxide layers formed on 70/30 cupro-nickel alloys in seawater. The use of AES was invaluable and in fact, there are few other surface analytical techniques available that can provide the information for adequate understanding of the growth of such thin layers. The ultra-high surface sensitivity is essential to detect the thin corrosion product layers that form during the early stages of corrosion, toward which this study was directed.

The origin of Auger spectra is shown in Figure 6. An electron in the core level of a surface atom is removed by an electron or x-ray beam in the 1-10 Kev range. The excited ion will decay to a lower energy state by electronic rearrangement, whereby a valence shell electron will replace the ejected core level electron, with ejection of another valence electron that carries away the excess energy.

Figure 6. Electronic Origin of Auger Electrons.



The second valence electron (Step 3) for this diagram is more commonly called a KLL Auger electron to signify that it is a part of a multielectron rearrangement process. Because the process is multistaged it will be very element specific, allowing unambiguous element identification.

Another important feature of AES is the surface sensitivity. The only way for the Auger electron to escape the solid without losing its energy by collision or by interaction with other atoms is if it originates at or near the surface. An escape depth on the order of a monolayer ( $\sim 10 \text{ \AA}$ ) is typical for most Auger transitions. Also, if there are a number of atoms of the same type at the surface, the probability of many Auger transitions will increase and more Auger electrons will be counted.

Thus, Auger analysis allows good surface resolution

and the ability to unambiguously identify the composition of surface layers. Detection limits will be from 0.02 to 0.2 atomic percent and precision can be as good as  $\pm 5\%$ , depending on how much care is taken to control parameters, making quantitative analysis certainly possible. Also, all elements above He in the Periodic Table have characteristic Auger spectra, increasing the method's versatility.

Electrons must be counted in a ultrahigh vacuum system ( $\sim 10^{-10}$  Torr) which can be a disadvantage for many in situ studies. Great care must be taken to assure the vacuum is not contaminated by polluting species such as organics or water vapor. Otherwise, the deposition of these materials upon the surface will occur in a matter of minutes. The elements of interest will be masked by contaminating species which must be removed before analysis can proceed.

Besides an ultrahigh vacuum system, the Auger instrument must have an electron gun for sample excitation and an energy analyzer for counting the number of electrons at various energies. Electronic signal processing and computer control are helpful accessories. Since Auger electrons counted at a certain energy ( $N(e)$  or counts) are superimposed on a continuous background of secondary electrons, peaks are more easily distinguished by differentiating the energy distribution function,  $N(e)$ , with respect to energy to give  $dN(e)/d(e)$  spectra. A typical Auger spectra for 70/30 cupro-nickel corroded in seawater is shown in Figure 7.

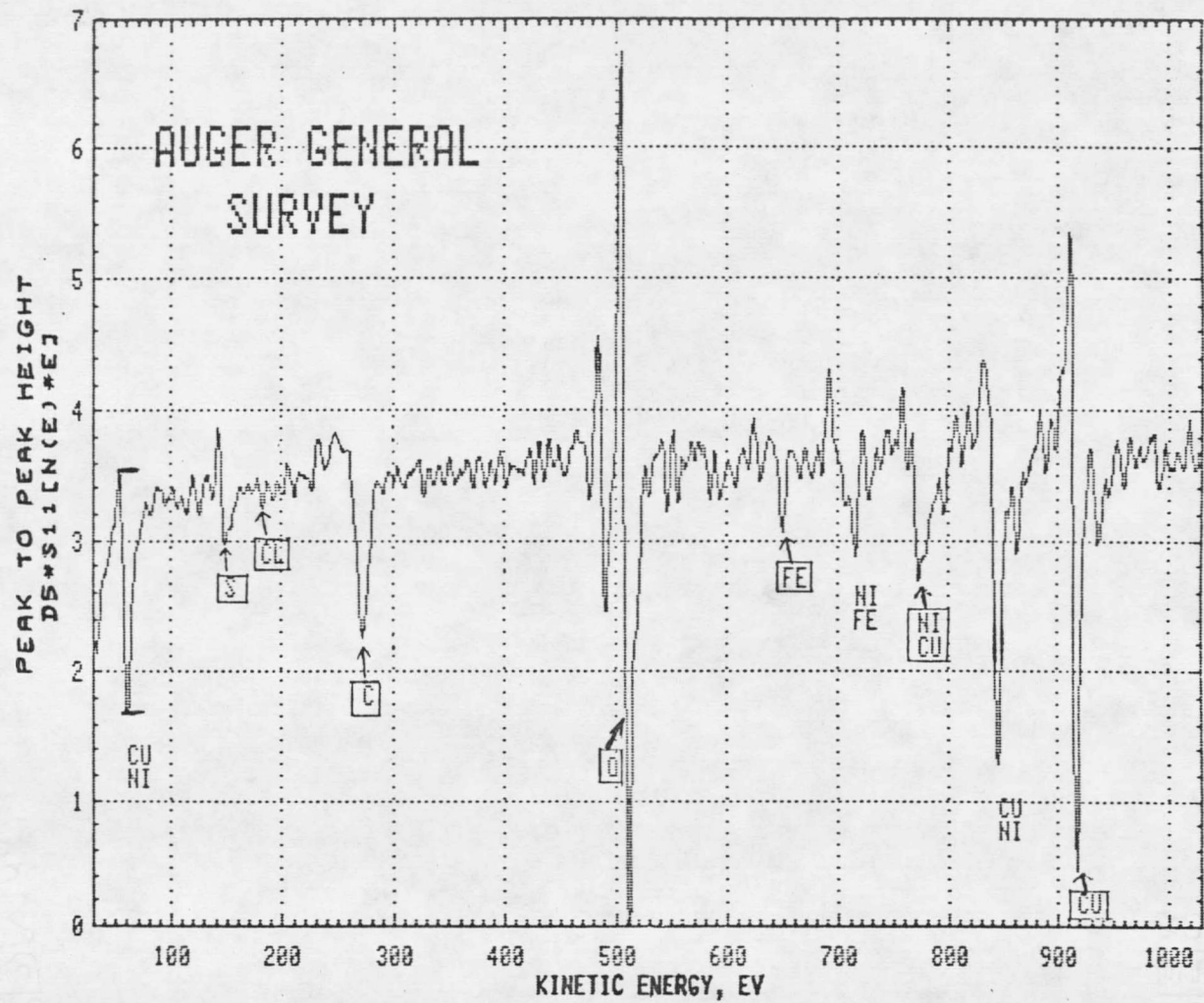


Figure 7. Typical Auger General Survey.

The principal energies used for this study are indicated by arrows. Quantitative data can be taken from the peak to peak distances as indicated by the horizontal bars. When the peak to peak height is divided by an appropriate, empirically determined sensitivity factor, then summed with similar data for other detectable elements, the atomic percent of that element can be calculated as shown in the following equation:

$$C_x = \frac{P_x/S_x}{\sum P_i/S_i} 100$$

where  $C_x$  is the atomic percent of element  $x$  and  $S_x$  is the sensitivity factor for the transition which is tabulated in the Auger spectra handbook,<sup>47</sup> relative to the Ag MNN Auger peak.  $P_i$  and  $S_i$  are the peak to peak distances and sensitivity factors, respectively, for the other  $i$  detectable elements.

In routine quantitative analyses, narrow energy regions are scanned and differentiated for calculation of atomic percents, without having to scan the entire energy spectrum. This time-saving mode of taking data is referred to as multiplex data and is used for most analytical features offered by the Auger instrument. There are several good references available concerning Auger Analysis of cupro-nickel alloys.<sup>48-51</sup> More details on general Auger theory can be found in References 47 and 52-55.



Depth Profiling:

Auger analysis would be somewhat limited in usefulness if depth profiling were not available. Because of the narrow escape depth of Auger electrons, the method is highly surface sensitive, however, sampling of the surface is restricted to only the top 10 to 20 Å. Most tarnish layers are many times that thickness so some form of etching away the surface, as Auger data is collected, is required. An Argon ion beam is scanned over the surface of the sample covering an area larger than the Auger analysis area. This will assure uniform removal of material within the analysis area. The beam mills away the surface as multiplex Auger data is collected until the tarnish layer is penetrated. The milling or sputter time is then plotted against atomic percent values calculated from the Auger data to provide the depth profile. If the etch rate is calibrated on a layer of known thickness, the sputter time can be related to actual depth, making the data more useful.

The use of the depth profile was invaluable to this study. Tarnish layers that formed on 70/30 cupro-nickel exposed to seawater for several days reached a limiting thickness of around 2000 Å. This thickness is easily analyzed in about 30 minutes milling time at moderate etch rates making the analysis experimentally feasible. If the layers were much thicker, however, too much time would be

required for analysis or else a very fast etch rate would be needed.

At the high energies required for fast etch rates, "knocking on" effects can occur. Argon ions penetrate the surface far enough to be retained and become part of the surface atom population. The resulting dilution by Argon lowers relative metal levels affecting the accuracy of the Auger analysis. Surface metal atoms can also be pushed or crowded into underlying layers resulting in concentration alteration.

Another problem associated with ion milling is preferential sputtering where one of the alloy components sputters away faster than another component. This results in enrichment of the latter component at the surface. A quantity called sputter yield is responsible. Sputter yield is the number of a particular atom removed from the surface per Argon ion collision and is a function of the atom's atomic weight and binding energy. For cupro-nickel alloys the following equation can be used to calculate surface concentration alteration due to sputter yield differences:<sup>50</sup>

$$N_s(\text{equilibrium}) = R N_b / (1 - N_b + R N_b) \quad (4)$$

where  $N_s$  and  $N_b$  are the surface and bulk alloy nickel compositions respectively, and  $R$  is the ratio of copper sputtering yield to nickel sputtering yield. As indicated, the equation applies at equilibrium. Equilibrium conditions

will be established if enough sputter time elapses, (usually within 5 to 10 minutes) allowing nickel surface atoms to reach a saturation level. The equation predicts a 45% Ni, 55% Cu surface composition at saturation for a bulk alloy composition of 70/30 Cu/Ni when  $R = 1.9$ . This value is obeyed for a 0.5 Kev Argon ion beam at a current density of 15-20  $\mu\text{A}/\text{cm}^2$ .  $R$  is insensitive to changes in the beam energy if energies above 150 eV are employed.<sup>51</sup>  $R$  is also insensitive to current density changes being 1.9 at 15-20  $\mu\text{A}/\text{cm}^2$  and 1.6 at 500  $\mu\text{A}/\text{cm}^2$ .<sup>48</sup> Changing the angle of incidence of the ion beam with respect to the sample surface also has little effect. The problem of preferential sputtering can be very serious since atomic percent data from the depth profiles will be inaccurate and independent of corrosion processes.

Although other researchers<sup>48-51</sup> reported preferential sputtering to be a problem with cupro-nickel alloys, the results of this study showed no surface composition alteration. Depth profile information indicated the surface metal composition remained the same as the bulk metal for very long sputter times (in excess of 1 hour) when analyses were performed on clean, uncorroded specimens of alloy. It is proposed that the difference in etch rates is responsible for the discrepancy. This work utilized a relatively high etch rate of 60  $\text{\AA}/\text{minute}$  for a 300  $\mu\text{A}/\text{cm}^2$  beam at 1.5Kv, compared to a maximum of 23  $\text{\AA}/\text{minute}$  for other studies.<sup>48,49</sup>

The ion beam alters the surface composition to a depth "d". If the Auger sampling depth is less than d then the Auger data will be affected by preferential sputtering. If the etch rate is very fast, (as for this work) material is removed too quickly for d to become significant and the Auger sampling depth will be greater than d. The equilibration requirement for the previous equation cannot be met. Thus, the Auger data for fast etch rates (in excess of 23 Å/minute) will not show the effects of preferential sputtering. Although unplanned, the lack of sputtering enrichment in this work was very fortunate and accurate data was obtained without realizing sputter yields could be a problem.

Calibration of etch rates was performed on 1000 Å SiO<sub>2</sub> on Si and 1500 Å Ta<sub>2</sub>O<sub>5</sub> on Ta wafers. The SiO<sub>2</sub> etch rate was very similar to the Ta<sub>2</sub>O<sub>5</sub> rate despite the differences in the two oxides. Thus, a similar rate was assumed for copper and nickel oxides. For simplicity, the sputter conditions were adjusted slightly to give an etch rate of 60 Å/minute so that the sputter time in seconds corresponded to thickness in Angstroms. Once the thickness and atomic percent axes of the depth profile were determined to be accurate, the depth profile information could be used to evaluate surface corrosion product layers with confidence.

Depth profiles of Cu, Ni, O, Cl, S, and C were routinely run on corroded samples. If all of these profiles

were placed on the same graph, confusion would result from all of the line crossings. Since the levels of Cl, S, and C were always at or below the detection limit they can be omitted from the profile graphs, relieving the confusion. The remaining profiles of Cu, Ni, and O were the most important, especially O, because oxide layers were the main corrosion product.

The oxide profiles can have a variety of shapes, as illustrated in Figure 8.<sup>55</sup> Type 1 profiles show an oxide plateau indicating a definite boundary between the oxide layer and underlying alloy. The presense of a plateau allows estimation of the stoichiometry of the oxide layer by comparing the height of the plateau to the copper level at the same depth. The thickness of the oxide layer can also be estimated by the location of Point C on the depth axis where the oxide level approaches the background. This shape was the most common of the profiles seen in this study.

If the surface of the sample is rough, the oxide layer will be difficult to remove with the Argon ion beam. As a result, the oxide profile will gradually taper off linearly to background levels. Profiles with this shape are classified as Type 2 profiles and are uncommon when good pretreatment procedures are used.

When corrosion conditions are adjusted to suppress corrosion product formation, or when exposure times are very short, Type 3 profiles will be seen. The only appreciable

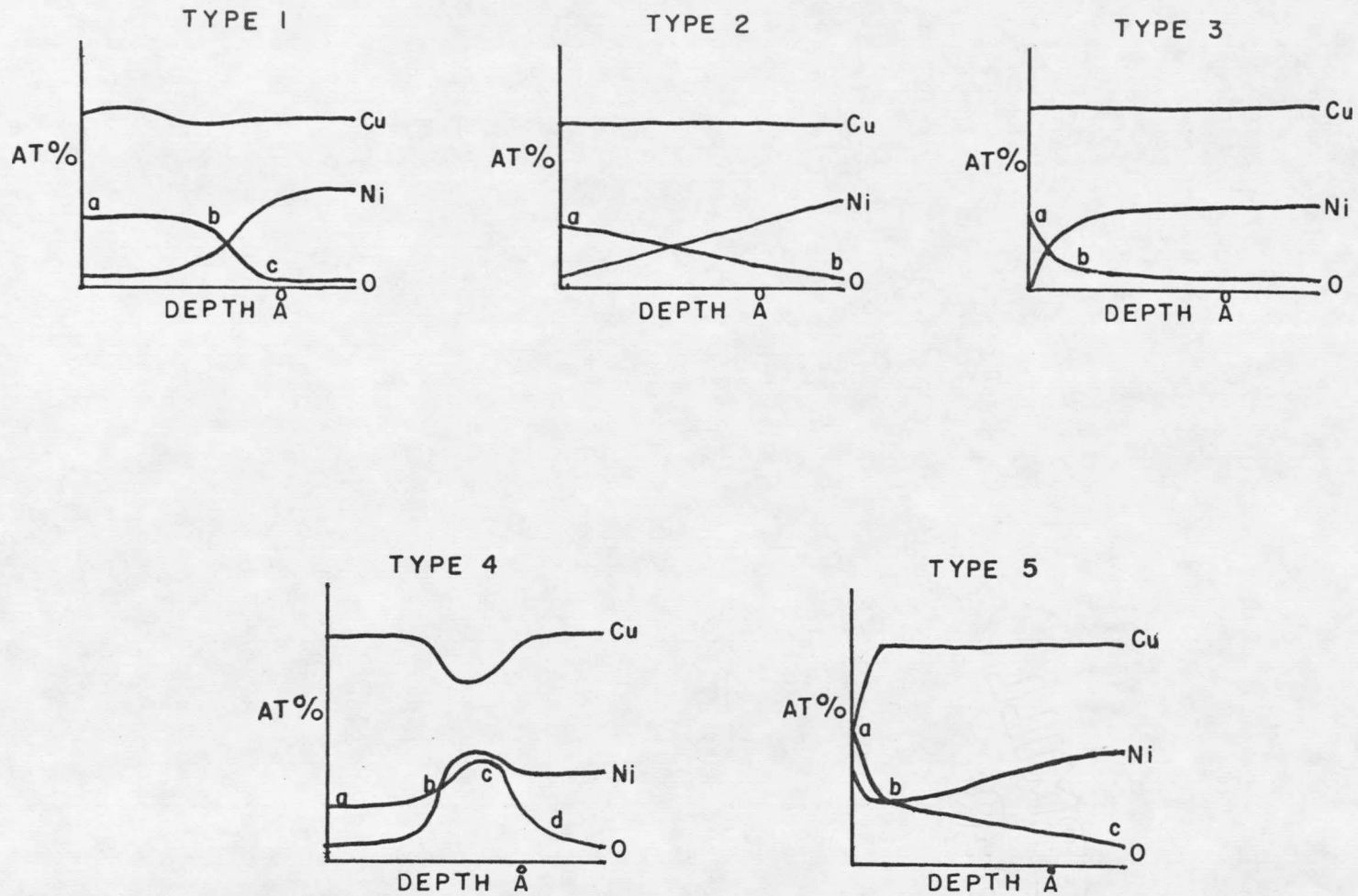


Figure 8. General Types of Auger Depth Profiles.

level of oxides is at the very surface located by Point A. One or two monolayers of oxide is sufficient to give this profile shape.

Type 4 profiles were the most complicated due to the reorganization of the oxide layer to higher levels of Ni. A two phase oxide layer is formed with copper oxide overlying nickel oxide as indicated by the dip in Cu levels. On longer term samples, the dip can grow and extend to the surface causing the profile to appear like a Type 1 profile with the Cu and Ni lines switched. The boundary between the two oxides is marked by Point B and the center of the nickel oxide layer is marked by point C. Samples exposed to seawater for more than a day showed nickel oxide extending to the surface by the loss of the Point A to B segment.

Type 5 profiles were typical of oxide layers that were two phase across the surface of the sample instead of into the sample. Samples that were treated with agar showed a very thin layer of nickel oxide surrounding much thicker islands or nodules of copper oxide. As soon as the thinner nickel oxides were removed (Point B), the nodules of varying size were removed gradually until background levels were reached (Point C). Sputter times in excess of 1 hour were sometimes required to reach Point C.

Depending on the experimental conditions, the depth profiles can be a combination of these shapes, making interpretation more difficult. However, the majority of

profiles can be classified as one of these types. These shapes will be referred to throughout the rest of the discussion and more detail will be given where appropriate.

One of the most important pieces of information obtained from the depth profile, besides layer thickness, is the area under the oxide profile. This value can be related to the weight of corrosion product (see mass balance derivation section) providing a good estimate of the tarnish layer growth. By using standard exposure times of 30 minutes, comparisons of oxide layers will give relative tarnish rates which can be evaluated for different experimental conditions. This simple rate determination method was used extensively throughout the parameter evaluation section to be presented. Relative areas ( $AT\%-\overset{\circ}{\text{A}}$ ) at 30 minutes exposure were plotted against each corrosion parameter to evaluate its effect on formation of a tarnish layer.

#### Other Features:

Other analytical features available on most Auger instruments include Scanning Electron Microscopy (SEM), element mapping, line analysis, and point analysis. The SEM allows precise imaging of the surface over which Auger data is taken allowing correlation of surface features with elemental analysis. Analyses can be taken over the entire surface shown on the SEM imaging screen or across a line drawn across the surface for relative element level



comparisons on surface features. Precise points can also be defined for analysis for exact feature identification. An element map across the surface can be made by defining a grid of point analyses and letting the atomic percent level at each point regulate the brightness of a dot placed at each analysis position on the screen. Photomicrographs can then be taken and correlated with surface features. All of these features were used to study the corrosion reactions of 70/30 Cu/Ni in seawater. More information on each feature will be given in the experimental section.

#### Material Balance

Electrochemical reactions that occur during corrosion of metals are complex and depend on the corroding medium and environmental conditions. Because of the complexity of these processes, any one analytical technique cannot provide enough data to understand the corrosion process.

Historically, most corrosion reactions were studied by electrode methods because the majority of corrosion reactions are electrochemical.<sup>56</sup> However, one of the disadvantages of electrochemical measurements is their interference with the corrosion reaction itself.<sup>57</sup> It must be assumed that a freely corroding metal will behave the same way as a metal placed in the electrochemical cell. With the recent development of several surface analytical techniques<sup>58</sup> coupled with more conventional corrosion

measurements, many corrosion reactions can be successfully studied. Electron Spectroscopy for Chemical Analysis (ESCA), also known as X-ray Photoelectron Spectroscopy (XPS), and Auger Emission Spectroscopy (AES), which has already been discussed, are the most popular surface techniques.<sup>59,60</sup> ESCA provides chemical state information with depth when ion milling is used to erode the surface away. Both ESCA and AES can only be used to evaluate the tarnish layers on the corroded metal, however, and cannot provide information about the overall corrosion process. Also, in situ corrosion analysis is impossible because of the ultra-high vacuum requirements of the techniques. Raman Spectroscopy has in situ capability, but may not be sufficiently sensitive.<sup>61,62</sup> It also has the advantage of being non-destructive to the sample being studied.

Any of the surface methods, when supplemented with material balance techniques, will provide a more detailed analysis of the corrosion process. Material balance accounts for all weight losses and gains with respect to the corroded metal and corroding medium. By using AES to analyze the corrosion product layer on the metal surface, Atomic Absorption Spectroscopy (AAS)<sup>63</sup> to determine metal levels lost to solution, and microbalance readings to monitor weight changes in the coupons, the data required for adequate understanding of the corrosion of cupro-nickel alloys in seawater can be generated.

The closed system used in this study (see experimental section) allowed easy monitoring of solution losses by AA. Other experimental designs where metal samples are exposed to open ocean waters or large volumes of seawater, will not be amenable to solution analysis due to the extreme dilutions and lack of containment. If analytical detection limits and interference levels are low, and containment of the used seawater is possible, the course of the corrosion reaction can be followed as it occurs by direct analysis of small aliquots of the corroding seawater for various exposure times. If detection limits and interferences limit the analysis, the procedure becomes much more complicated since direct analysis cannot be performed. One method of eliminating interferences and improving detection limits at the same time is to pass the used seawater over an ion-exchange resin column which rejects interfering species like major seawater ions, and retains the metals of interest. The metals can then be eluted with a small volume of acid and analyzed on the AA. Once the total level of weight losses to solution are known, by microbalance readings, the amounts of metal not recovered by the resin can be calculated, completing the solution analysis.

The best ion-exchange resins to use are Chelex-100 (Bio-Rad Labs, Richmond Ca.) and Dowex A-1 (Dow Chemical), the latter being an impure form of Chelex-100. Both resins have a styrene lattice with iminodiacetic acid groups that have a

high affinity for heavy metals such as Cd, Cu, and Ni, and a low affinity for Na, Ca, and Mg. As long as the pH is kept above 5, Cu and Ni ions will be quantitatively removed from solution at recoveries better than 96% and over 99% of the major seawater species will be rejected. The method is patterned after a paper by Riley and Taylor<sup>64</sup> who used the procedure to determine background levels of heavy metals in various seawaters. The method works equally well for Cu and Ni introduced by corrosion and forms a key part of the mass balance procedure. Several precautions must be taken, however, if the metal species are in non-retainable form.<sup>65,66</sup> Precipitated metal or insoluble metal complexes will not be removed by Chelex-100 and errors will occur if the method is used to determine total metal background levels. This is an advantage for this study since it allows calculation of insoluble corrosion products lost to solution.

Once solution data, Auger data on the tarnish layers, and mass loss data from microbalance readings are collected, they are entered into the material balance equations presented in a following chapter. The equations predict the fate of each metal species involved in the corrosion process as well as the role of oxygen in the tarnish reactions. Due to the complexity of the mass balance procedure, a more detailed discussion of the method is warranted and will be presented in subsequent chapters. The material balance is one of the most important parts of this study.

### Biofilm and Organic Gel Properties

The previous discussion on general corrosion behavior pointed out the importance of biofouling and other forms of fouling on the cupro-nickel corrosion process. A discussion of the physical properties of biofilms and "synthetic biofilms", such as organic gels (agar-agar and gelatin), is appropriate and leads the way to answering the questions of how and why an organic layer affects corrosion. Once the physical effects on corrosion are determined, the chemical effects due to specific corrosive byproducts originating from a viable biofilm can be singled out. This will be one of the major applications of this study.

#### Biofouling Processes:

In order to understand the properties of a biofilm a knowledge of the structure and changes in the structure during the establishment and growth periods is required. Figure 9 summarizes the major processes of biofilm formation in chronological order from left to right.

When a cupronickel alloy is placed in natural seawater, it rapidly forms its protective oxide layer before any significant biological activity can be established. The relatively inert oxide layer then becomes the substrate for the biofilm to form upon. Growth then proceeds in five consecutive stages:<sup>67</sup>

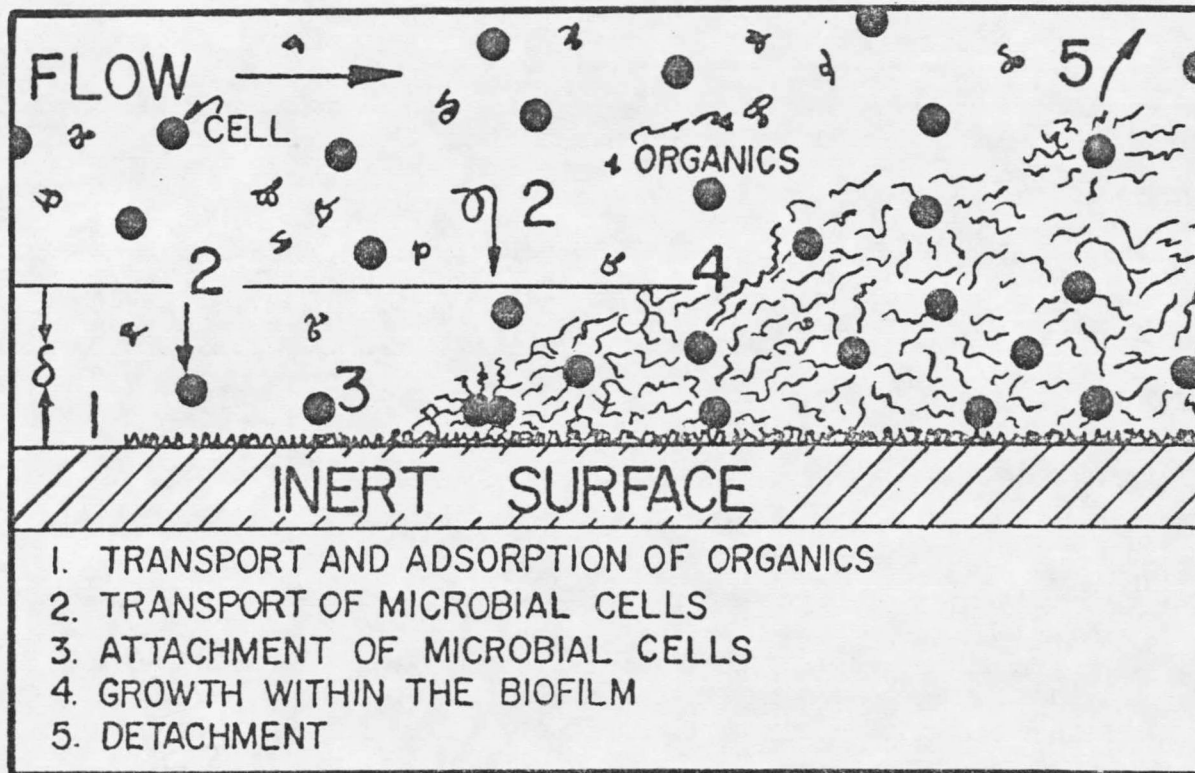


Figure 9. Biofilm Growth Stages.

- (1) Transport and adsorption of organic macromolecules on the inert surface.
- (2) Transport of microbial cells to the surface.
- (3) Attachment of microbial cells.
- (4) Multiplication of cells and formation of extra-cellular material.
- (5) Detachment or spalling of material due to shear forces of flowing seawater.

The first stage is reported to occur within the first few minutes of exposure to natural waters containing nutrients, microorganisms, and organic macromolecules such as glycoproteins and polysaccharides. These molecules will adsorb to an inert surface at a rate not greater than 0.5 nm/minute and will reach a limiting thickness of less than 0.1  $\mu\text{m}$ .<sup>68</sup> There is, undoubtedly, some effect on the adsorption rate due to continual renewal of the surface by oxide layer formation during initial exposure to seawater. Some time may have to pass before the surface is "inert" enough for an organic layer to be established. Since establishment of this organic layer is thought to be a precursor of a developing biofilm, the formation of a biofilm may have to wait until sufficient oxide layer has formed. Although it is very important, the question of how the oxide layer formation affects the deposition of an organic layer and biofilm is unanswered at this point. This study strived to answer part of the opposite question, i.e., how does a biofilm affect the corrosion process?

Once it forms, the organic layer will have a thickness that is too small to have a significant effect on the heat transfer or fluid flow characteristics at the surface. This will continue to be the case as long as the layer is thinner than the laminar sublayer thickness. The layer will, however, alter the surface properties of wettability, surface tension, and electrophoretic mobility in such a way that a specific microbial cell finds the surface hospitable.

Colonization of the surface by rod-shaped pioneer bacteria such as *Flavobacterium*, *Achromobacter*, and *Pseudomonas* then occurs as represented by stages 2 and 3. The cells are brought near the surface by turbulence or chance and enter the thin boundary flow layer having a thickness  $d$ . (The calmer conditions in this area give a cell a chance to attach to the surface if it touches the surface.) The cell will adhere reversibly by electrostatic attraction, interfacial tension, covalent bonding, or Van der Waals forces which are influenced by the surface characteristics. Since the preadsorbed organic layer affects the surface characteristics, its role is more clear. The surface properties are also influenced by multivalent cations such as  $\text{Ca}^{+2}$ ,  $\text{Mg}^{+2}$ , and  $\text{Fe}^{+3}$ , which are commonly found in seawater. These ions are complexed with surface organic macromolecules, altering the overall surface layer.

Held under the actions of these surface forces, the cells can be easily removed by downward turbulent bursts in



the boundary layer. If there are no appreciable lift forces available, the cell will roll along the surface until it reattaches. If, by chance, it remains in one place long enough, extracellular polysaccharides will be produced by the cell forming a permanent or irreversible form of adhesion to the surface.

Once the cells are firmly attached, they extract nutrients and energy from breakdown of organic or inorganic compounds and undergo growth, reproduction, maintenance, and extracellular product formation. These processes are illustrated as stage 4 in Figure 9. The usual growth pattern involves formation of a network of connecting fibers of extracellular material which give the film a rigid structure. Silts and sediments, if present, will be captured, adding to the density and lowering the permeability. If the layer becomes thick enough or impermeable, diffusion limitations will cut off the supply of nutrients and oxygen to lower layers resulting in death or lysis of the underlying cells. Selective establishment of anaerobic organisms such as Thio-bacillus Thiooxidans, that derive their energy from reducing inorganic ions like  $SO_4^{2-}$ , will usually occur, leading to changes in the film's structure. The resulting loss of adherence under the influence of shear forces of the flowing seawater will lead to spalling or removal of the biofilm in patches. Also, if the layer becomes thick enough and extends above  $d$ , shear forces can be excessive resulting in "tearing

away" of the upper parts of the layer, as shown by stage 5. If scavengers such as Flavobacterium or Agarbacterium proliferate, the polymer structure can be dissolved since these species are actively proteolytic. The loss in structural integrity can result in further spalling.

Whether the layer undergoes lysis in the lower regions or is torn away by shear forces, it will reach a limiting thickness in the 0 to 1000 um range in a matter of days or weeks. The net growth rate will be determined by flow, temperature, oxygen availability, and nutrient levels. The layer will also have a structure that can be physically characterized and approximated by artificial means (agar) as will be discussed shortly.

The influence of corrosive cellular byproducts or oxygen deprivation due to cell metabolism will be considered direct effects of the biofilm on corrosion processes. The physical presence of a biofilm and the associated hindrance to mass transfer will be considered as indirect effects on corrosion and are the main topic of this study.

#### Biofilm Properties:

As a biofilm forms, it acquires many easily measured properties that characterize the film.<sup>69</sup> The various properties that can be determined are summarized in Table 3 which indicates directly measureable properties and properties that must be inferred from direct measurements.

Table 3. Measureable Properties of Biofilms.<sup>69</sup>


---

 Direct Measurement:

Thickness	Biofilm Fiber Count
Mass	

## Indirect Measurement:

Frictional Resistance to Flow	
Density	Heat Transfer Resistance
Mass Transfer Resistance	(Diffusion)

## Constituents:

Polysaccharide	Nucleic Acid
Organic Carbon	Protein
Chemical Oxygen Demand (COD)	

## Viable Cell Constituents:

Viable Cell Count	Lipopolysaccharide
Adenosine Tri-Phosphate (ATP)	

---

The properties of particular interest to this study include thickness, mass, density, fiber count, and mass transfer resistance, because they determine the corrosion behavior due to the mere presense of a nonviable layer. These characteristics can be approximated by a synthetic organic gel layer, allowing fast evaluation of corrosion properties without growing real biofilms in the laboratory. Methods for measuring the properties of Table 3 can be found in Reference 70, Chapters 9 and 11.

Thickness is perhaps the most important biofilm property to measure since it helps define how much resistance there is to flow, mass and heat transfer, and corrosion properties.

























































































































































































































































































































































































































































































































































































































































































































































































